Chinese Physics Letters **40**, 122101 (2023) **Review**

Phase Transition Study Meets Machine Learning

Yu-Gang Ma(马余刚)[1,2*], Long-Gang Pang(庞龙刚)[3*], Rui Wang(王睿)[1,4,5*], and Kai Zhou(周凯)[6*]

[1]*Key Laboratory of Nuclear Physics and Ion-beam Application (MOE), and Institute of Modern Physics, Fudan University, Shanghai 200433, China*
[2]*Shanghai Research Center for Theoretical Nuclear Physics, NSFC and Fudan University, Shanghai 200438, China*
[3]*Institute of Particle Physics and Key Laboratory of Quark and Lepton Physics (MOE), Central China Normal University, Wuhan 430079, China*
[4]*Shanghai Institute of Applied Physics, Chinese Academy of Sciences, Shanghai 201800, China*
[5]*INFN Sezione di Catania, 95123 Catania, Italy*
[6]*Frankfurt Institute for Advanced Studies (FIAS), D-60438 Frankfurt am Main, Germany*

(Received 10 October 2023; accepted manuscript online 9 November 2023)

In recent years, machine learning (ML) techniques have emerged as powerful tools for studying many-body complex systems, and encompassing phase transitions in various domains of physics. This mini review provides a concise yet comprehensive examination of the advancements achieved in applying ML to investigate phase transitions, with a primary focus on those involved in nuclear matter studies.

DOI: 10.1088/0256-307X/40/12/122101

1. Introduction. As a foundational concept in the exploration of many-body physical systems, phase transitions encapsulate phenomena as commonplace as the freezing of water into ice and as esoteric as the postulated quark–gluon plasma to hadronic matter transition believed to have occurred in the early universe or during heavy-ion collisions. Phase transitions across these various physical domains share fundamental similarities, primarily characterized by a drastic change in the state of matter due to thermal fluctuations and/or quantum effects. Universal features such as critical exponents and symmetry breaking forge a connection among disparate systems, enabling the transference of insights and methods across disciplinary boundaries. Nevertheless, each physical system brings with its unique challenges and intricacies. Specifically, research of the phase transitions of nuclear matter governed by quantum chromodynamics (QCD) is crucial to our understanding of the nature of strong interactions and has burgeoned into a pivotal research area.[1,2] This includes explorations of, e.g., nuclear liquid–gas phase transition,[3–10] as well as the phase structure of hot and dense QCD matter.[11–13] However, the non-perturbative nature of QCD, especially at low energies, makes information about phase transitions particularly elusive, often surpassing the capabilities of traditional theoretical methods. In general, studying phase transitions in complex systems, especially those with many degrees of freedom, usually poses significant computational hurdles. In this context, machine learning (ML) techniques[14–21] offer novel and promising investigation pathways.

This short review aims to elucidate the synergies between ML[22–28] and phase transition studies, and how these interdisciplinary collaborations are paving the way for new insights in physics. We delve into recent breakthroughs where ML methods, including supervised and unsupervised learning, have been applied to phase transition studies of nuclear matter, enabling a finer characterization of the QCD phase diagram and a deeper understanding of the nuclear matter properties. We also discuss the challenges and future directions in this exciting and rapidly evolving field.

2. Phase Transition in Condensed Matter Physics.

2.1 Supervised Learning and the Ising Model. The first application of ML techniques to phase transitions emerged in the field of condensed matter physics.[29] ML techniques are designed to characterize complex datasets, which makes these techniques particularly suitable for recognizing and classifying the phases of matter. Here, we take the example of employing a fully connected neural network [the inset in Fig. 1(a)] to the square-lattice ferromagnetic Ising model ($H = -J\sum_{ij}\sigma_i^z\sigma_j^z$, with J being the interaction and $\sigma_i^z = \pm 1$ the spin). The dataset used for training and testing the neural network consists of two-dimensional spin configurations sampled by Monte Carlo simulations for different temperatures T. The neural network was trained to classify the ferromagnetic configurations (below critical temperature T_c) and the paramagnetic configurations (above T_c). Figure 1(a) shows the output of the neural network averaged over a test set as a function of T/J for different system sizes represented by L. Clearly, the trained neural network could respond differently to spin configurations with low temperatures and those with high temperatures. The temperature at which the two outputs are equal to each other, namely the crossing temperature T^*, can be viewed as the T_c obtained by the neural network for the particular L. In the language of renormalization, one can rescale those T/J dependences of the output, i.e., $T/J \to tL^{1/\nu}$ with $t = (T - T_c)/J$,

*Corresponding authors. Email: mayugang@fudan.edu.cn; lgpang@mail.ccnu.edu.cn; rui.wang@ct.infn.it; zhou@fias.uni-frankfurt.de
© 2023 Chinese Physical Society and IOP Publishing Ltd

to obtain the critical exponent $\nu \approx 1.0 \pm 0.2$ [Fig. 1(b)]. With the $1/L$ dependence of T^*/J shown in Fig. 1(c), by taking the limit $L \to \infty$, one can obtain the crossing temperature from the neural network $T^*/J = 2.266 \pm 0.002$, which estimates quite accurately the physical critical temperature of the square-lattice Ising model. The latter can be obtained theoretically in the thermodynamic limit, i.e., $T_c/J = 2/\ln(1+\sqrt{2})$.

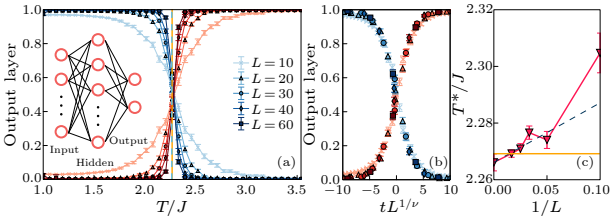

Fig. 1. (a) Output of the neural network averaged over a test set as a function of T/J. The input of the neural network is the two-dimensional spin configuration of the square-lattice ferromagnetic Ising model generated by Monte Carlo simulations. Different system sizes L are used. The inset shows the sketch of the neural network in use. (b) Rescaling of the output in (a) as $T/J \to tL^{1/\nu}$ with $t = (T - T_c)/J$. With proper ν, these lines can collapse into each other. (c) Plot of the finite-size scaling of the crossing temperature T^*/J (down triangles). The horizontal line represents the theoretical critical temperature in the thermodynamic limit $T_c/J = 2/\ln(1+\sqrt{2})$. Taken from Ref. [29].

Neural networks are even able to generalize the tasks beyond their original design. For the trained neural network in the case of the square-lattice Ising model, when fed with the spin configurations obtained by Monte Carlo simulations of the triangular-lattice ferromagnetic Ising Hamiltonian, the neural network successfully estimates the critical temperature $T_c/J = 3.65 \pm 0.01$ and $\nu \approx 1.0 \pm 0.3$, which are consistent with the theoretical values. Using a more complicated convolutional neural network, it is even possible to encode basic information about unconventional phases, such as those present in the square-ice model and the Ising lattice gauge theory, as well as the Anderson localized phases.[29]

2.2 Semi-supervised and Unsupervised Learning. Besides the supervised learning technique given in Ref. [30], a confusion scheme combining supervised and unsupervised learning has been proposed to classify the phases of matter. The main idea of the confusion scheme is as follows. First, classify the dataset with a proposed critical point u_c'. Then, supervised learning, such as the fully connected network, is applied to the dataset to obtain the test accuracy of the trained neural network for each u_c'. The test accuracy, as a function of u_c', will exhibit a W shape and the true critical point corresponds to the middle peak of the W shape. Since in this confusion scheme one does not require the knowledge of the order parameters, the topological content of the phases, or any other specifics of the transition in question, it provides a generic tool for identifying unexplored phase transitions.

Another well-known ML technique for studying the phase transitions in condensed matter physics is the auto-encoder method,[31,32] which is a pure unsupervised learning technique. The auto-encoder neural network has a mirror structure. The encoder part encodes the input layer into one or more latent variables and the decoder part decodes the latent variables to the output layer. The neural network is trained to best recover the encoded information, i.e., the network is trained to minimize the difference between the input layer and the output layer. The auto-encoder method has been shown to be a very effective algorithm for examining phase transitions for several typical models in condensed matter physics, such as the ferromagnetic Ising model and the XY model.[31,32]

3. Nuclear Temperature. One of the difficulties in studying the nuclear liquid–gas phase transition of nuclear matter arises mainly from the preparation of a finite-temperature nuclear system and the determination of its temperature. Heavy-ion collisions (HICs) provide a possible avenue for studying the finite-temperature properties of nuclear matter. During the collision reaction, a transient excited system is formed, which can be generally regarded as a (near) equilibrium state, since the evolution of its constituent nucleons is sufficiently short compared to the global evolution. Its temperature can be obtained from, e.g., energy spectra by moving source fitting, excited state populations, (double) isotope ratios or quadruple momentum fluctuations. For a brief review, see Ref. [33]. A reliable thermometer of HICs needs to be insensitive to both the collective effects and the secondary decay of unstable nuclei after the system disintegrates, which is generally difficult to achieve. Moreover, because of the difficulty in verifying the accuracy of the apparent temperature ($T_{\rm app}$) obtained by these thermometers, it is not a trivial task to propose different ways of determining $T_{\rm app}$ and thus provide more opportunities for cross-checking.

Using ML techniques, the charge multiplicity distribution can be used to determine $T_{\rm app}$ of HICs at intermediate-to-low energies.[34] Usually, the fragment charge distributions $M_c(Z_{\rm cf})$ show typical changes of the hot nuclei disassembly mechanism with temperature, i.e., from an evaporation mechanism at a lower temperature, to multifragmentation at intermediate temperature, until vaporization at higher temperatures.

A relation between the source temperature of the model $T^{\rm model}$ and $M_c(Z_{\rm cf})$ can then be established by a deep neural network (DNN) that transforms the complex relation into a nonlinear map through its neurons. This relation can be used to determine $T_{\rm app}$ of a particular transient state during HICs at intermediate-to-low energies. With the final state charge multiplicity distribution simulated with an isospin-dependent quantum molecular dynamics, its apparent temperature is obtained by the trained DNN.

With the $T_{\rm app}$ determined by the DNN, the caloric curve, i.e., $T_{\rm app}$ as a function of the excitation energy per nucleon (E^*/A) of the HICs, is also examined. Traditionally, the characteristic behavior of the caloric curve is explained by the fact that, as E^*/A increases, the system is driven into a spinodal region, in which part of E^*/A begins to transfer to latent heat. From the simulation, the

extracted $T_{\rm app}$ at the maximum of the specific heat capacity of the system $\tilde{c} \equiv d(E^*/A)/dT_{\rm app}$, which is called the limiting temperature $T_{\rm lim}$, follows the general trend of Natowitz's limiting-temperature dependence on the system size[6] and thus indicates the validity of determining $T_{\rm app}$ through the charge multiplicity distribution with the help of ML techniques.

4. Nuclear Liquid–Gas Phase Transition. As mentioned above, ML techniques can be used to study nuclear temperature and then the caloric curve, which is of particular interest in reaction dynamics. Many sophisticated probes that analyze the information of the reaction products have been proposed to recognize the liquid–gas phase transition of nuclei.[3–10] Recently, a specific effect from initial-state α-clustering configurations[35–39] on the nuclear liquid–gas phase transition was also discussed.[40] Since the nucleus is an uncontrollable system, its liquid–gas phase transition is realized by tracing the effect of the spinodal instability on the reaction dynamics, e.g., by measuring the properties of the intermediate mass fragments (with charge number greater than 3).

In a recent work, the averaged charge multiplicity distribution $\langle M_{\rm c}\rangle(Z)$ of the quasi-projectile (QP) fragments in the reactions of ^{40}Ar on ^{27}Al and ^{48}Ti at 47 MeV/nucleon has been used to study the nuclear liquid–gas phase transition by the autoencoder method and a confusion scheme.[41] The QP fragments are supposed to come from the excited projectile nucleus, which can largely avoid the effect of dynamical evolution. They can be obtained by a three-source (i.e., a QP source, an intermediate velocity source, and a quasi-target source) reconstruction method.[7]

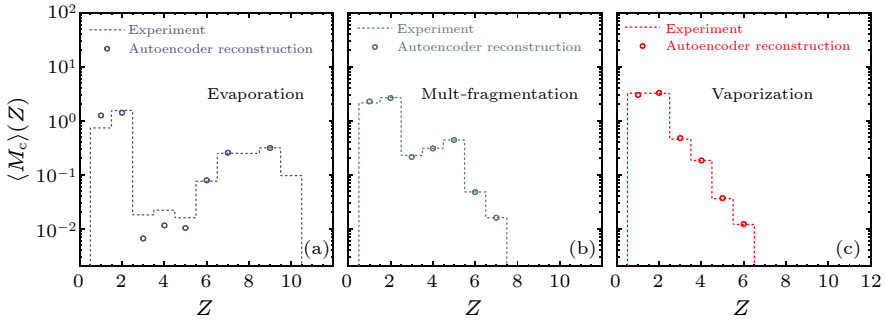

Fig. 2. The averaged charge multiplicity distribution $\langle M_{\rm c}\rangle(Z)$ of the QP fragments. The average is taken for different E^*/A bins, left panel for low excitation (0.9 MeV–2.8 MeV), middle panel for intermediate excitation (5.3 MeV–5.4 MeV), and right panel for high excitation (8.1 MeV–13.0 MeV). The dashed curves represent $\langle M_{\rm c}\rangle(Z)$ from the NIMROD experiment, while the circles are from the autoencoder network reconstruction $\langle M'_{\rm c}\rangle(Z)$. Each E^*/A bin contains 500 test events. Taken from Ref. [41].

The event-by-event charge-weighted charge multiplicity distribution of QP fragments $ZM_{\rm c}(Z)$ from the experiment is used as the input to train the autoencoder network. The network consists of two main parts: the encoder part encodes the input event-by-event $ZM_{\rm c}(Z)$ into a *latent variable* and the decoder part decodes the latent variable into $ZM'_{\rm c}(Z)$. The neural network is trained to recover the encoded information as best as possible, i.e., the network is trained to minimize the difference between $ZM_{\rm c}(Z)$ and $ZM'_{\rm c}(Z)$. Figure 2 shows the averaged $M_{\rm c}(Z)$ in three typical E^*/A bins (dashed lines). For the test QP events, the reconstructed $M'_{\rm c}(Z)$ are averaged and compared with the original $M_{\rm c}(Z)$ in Fig. 2. Once the autoencoder network is trained, each QP event is mapped to the latent variable. The latent variable as a function of $T_{\rm app}$ and E^*/A shows a sigmoid pattern, indicating that the trained autoencoder network treats the low and high temperature (or low and high excitation energy) regions differently. The area in the middle of the two phases represents those liquid–gas coexistence events that enter the spinodal region and are affected by the spinodal instability.

The confusion scheme mentioned above has been adopted to obtain the limiting temperature of the nuclear liquid–gas phase transition. The neural network is trained with the event-by-event charge-weighted charge multiplicity distribution of QP fragments $ZM_{\rm c}(Z)$ that is labeled according to a proposed limiting temperature $T'_{\rm lim}$. The phase transition properties can be deduced from the performance curve, i.e., the total test accuracy as a function of the proposed $T'_{\rm lim}$ of the neural network. The total test accuracy reaches its minimum at $T'_{\rm lim} \approx T_{\rm lim}$. The limiting temperature through the confusion scheme is 9.24 ± 0.04 MeV, which is consistent with the 9.0 ± 0.4 MeV obtained from the traditional analysis of caloric curve.[42]

5. Transition Identification in High-Energy HICs. It is conjectured that at high temperature and (or) density, QCD matter may experience a deconfinement transition where normal nuclear matter or hadron resonance gas would turn to a new state of matter, called quark—gluon plasma. There are two types of deconfinement phase transitions relevant to QCD: one is a crossover transition at vanishing or relatively small baryon chemical potentials and the other is a first-order phase transition at high baryon chemical potentials. The point at which these two types of transitions meet in the QCD phase diagram is called the critical point.[43–46] The first-principles lattice QCD study currently only has an achievable prediction for the QCD phase diagram in high-temperature and low-baryon chemical potential regions, while in high-density regions the calculation is hindered by the fermionic sign problem. As the only way on Earth to heat and compress nuclear matter for creating and studying QCD phase

transitions, HICs involve a complex and superfast evolving process, where though interesting physics including color deconfinement, which may indeed have occurred in the early stage during the collision, the excited fireball quickly expands with the temperature soon dropping to the confinement region. Therefore, experimentally, one can only resolve the finally emitted hadrons from HICs.

5.1 Convolutional Neural Network Based Identification of QCD Transition. With merely the final state pions' spectra, a deep learning-based equation of state (EoS) meter was proposed to identify the QCD transition type that occurs in the early stage of HICs.[47] At the level of relativistic hydrodynamics, binary classification of QCD transition, in crossover or first order, is performed by a convolutional neural network (CNN) with the final state pion's spectra as the input. See Fig. 3 for a demonstration. As a supervised learning task, the dataset can be generated from the well-developed hydrodynamic simulation for HICs, with the labels provided by the implemented two classes of EoSs, including either crossover or first-order transition type, in each generated collision event. The trained CNN shows above 95% event-by-event classification accuracy, which is also robust against different initial fluctuations and shear viscosities, indicating that information about the QCD transition that happened in the early time of HICs is not fully washed out by the evolution and still encoded in the final state, and can be decoded with CNN to help identify the phase transition with experimental measurements.

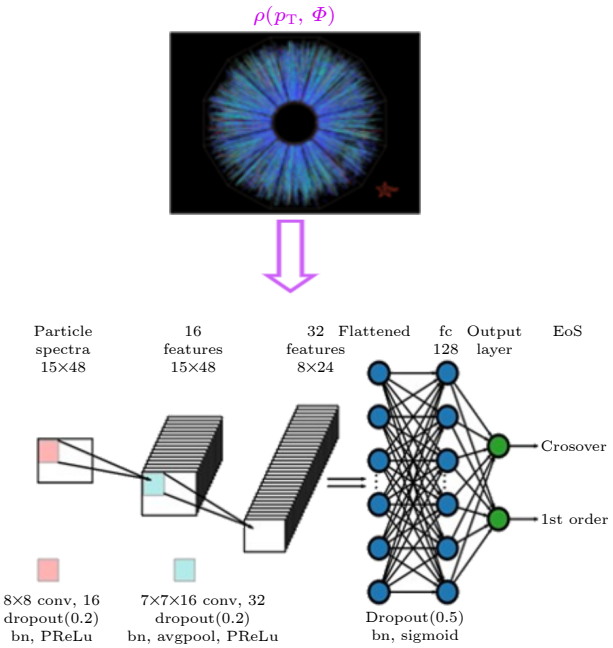

Fig. 3. Flowchart of QCD phase transition identification with heavy-ion collision particle spectra.

5.2 Extending the Classifier to Realistic Cases. This strategy was further extended to more realistic cases, e.g., including the afterburner hadronic cascade evolution via UrQMD simulation into the simulation in the transition identification,[48] where particlarization, hadronic rescattering and more stochasticity appeared inside the dynamics. The classification accuracy for the QCD transition type from the CNN indeed decreased on an event-by-event basis. However, it was demonstrated that with a fine-centrality-bin average the classification can be well achievable by the CNN. The non-equilibrium phase transition scenario was also discussed via introducing spinodal decomposition induced baryon clumping into the simulation for the classification task.[49] While in position space the CNN can easily distinguish a non-equilibrium transition from a normal Maxwell reconstructed transition inside the EoS, it struggles when only a momentum space spectrum is available. However, a PointNet-based model could provide a slight improvement, indicating that the characteristic of the two classes exists on an ensemble level. Moreover, the analysis was recently extended to directly use the experimental detector readout, where the PointNet-based model was accordingly explored to identify the QCD transition type for the Compressed Baryonic Matter experiment.[50]

6. EoS Study from HICs. In the context of HICs, the EoS of nuclear matter, which essentially encodes the QCD phase diagram and transition information, has long been one of the holy grails of both theoretical and experimental research. From a theoretical perspective, the EoS is a crucial input in our physical modeling for HICs, directly influencing the dynamical evolution of the collisions. As for dense isospin-asymmetric nuclear matter, which is expected to be produced in low-to-intermediate energy HICs, its density-dependent EoS is currently not understood and not accessible for first-principles lattice QCD calculations.

6.1 CNN Constrain Symmetry Energy. One way to generally characterize dense nuclear matter is using nuclear empirical parameters defined from a series expansion around the isospin asymmetry.[23,51–53] Among them, nuclear symmetry energy is critical in encoding the energy cost to make the matter more neutron rich. It is thus intriguing to obtain effective constraints over the nuclear symmetry energy with measurements in HICs. However, these measurements currently lack the sensitivity to provide inferences of the high-density part with a final state particle distribution. Applying a CNN to the final state proton spectra,[54] it was demonstrated that the types of nuclear symmetry energy can be reasonably classified and the slope parameter can be well identified under regression training.

6.2 Bayesian Inference of Dense QCD Matter EoS. Recently, for the first time, Bayesian inference was performed to constrain the density dependence of the nuclear matter EoS using observables from HICs in the beam energy range $\sqrt{s_{\rm NN}} = 2 - 10\,{\rm GeV}$.[55] Specifically, the elliptic flow and mean transverse kinetic energy of protons were used in the analysis, which provide tight constraints on the EoS of up to four times the nuclear saturation density. As a robustness check for predictability, the extracted EoS generates good agreement with other observables (the directed flow and differential elliptic flow) that are not used in the Bayesian analysis and also showed a comparable speed of sound constrained from neutron star observations.[56]

7. ML Phase Transition in Lattice Quantum Field

Theory. Besides experimental studies, phase transition can also be studied by lattice quantum field theory (QFT), where configurations of the many-body system can be simulated via Monte Carlo techniques to further evaluate different observables and partition functions.

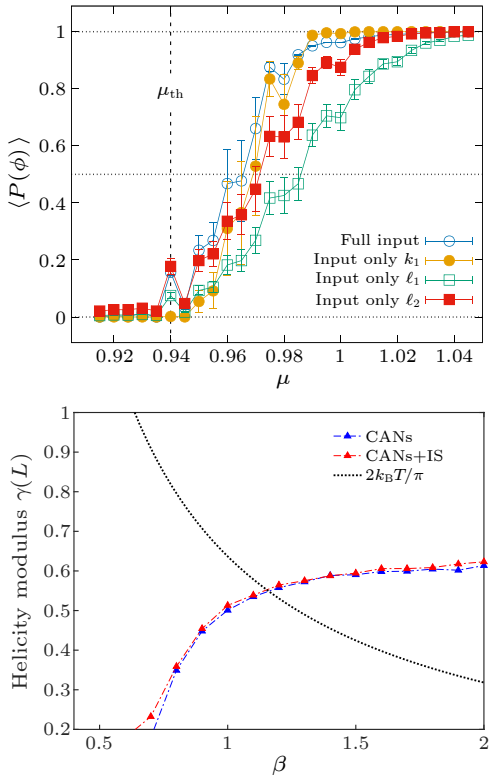

Fig. 4. Upper: the average condensation $\langle P(\phi)\rangle$ as a function of the chemical potential μ using full and restricted field inputs. Taken from Ref. [57]. Lower: the helicity modulus of a 2D XY model from CANs and CANs+IS cross with the curve $2k_{\rm B}T/\pi$ to derive the transition point, $\beta_{\rm c} \simeq 1.1796$. Taken from Ref. [58].

7.1 CNNs and Generative Adversarial Networks (GANs) for Scalar Field Study. Phase identification for the (1+1)-dimensional complex scalar field was explored[57] based on microscopic field configurations. For the considered system, the "silver blaze" behavior is expected, where the particle density will be suppressed at low chemical potential until some threshold $\mu_{\rm th}$. It will then increase considerably and enter a condensation region. A CNN was trained to identify the condensation phase with a training set consisting of only two ensembles of field configurations: one well above and one well below the transition chemical potential $\mu_{\rm th}$. After training, the testing was performed on ensembles of configurations at different chemical potential values in between the two training chemical potential values. It was found that the ensemble average of the network output serves as an accurate phase classifier, $\langle P(\phi)\rangle$, with its non-vanishing point along with increasing chemical potential precisely indicating the transition point (see the upper panel of Fig. 4). Physical observables such as the order parameter of the system–particle density n and the squared field $|\phi^2|$ were also shown to be capable of being regressed well with the CNN. The authors of Ref. [57] further discussed using GANs to provide a fast, efficient sampler for independent field configuration generation. It demonstrated the ability to capture the underlying statistical distribution of configurations for the system and thus also obtained the partition function.

7.2 Variational Autoregressive Generation of Field Configurations. Deep generative models in ML provide an efficient way to study the phase structure of statistical many-body systems, which could replace or assist the conventional Markov chain Monte Carlo simulation in related studies. Recently, a variational approach with an autoregressive network[59] was devised to solve Ising systems. The approach can be viewed as an extension of the mean field approach, where the variational ansatz is represented by more flexible neural networks. To generalize the strategy to many-body physics systems with continuous variables, the authors of Ref. [58] introduced the Beta distribution layer and a wave-net structure to construct a continuous autoregressive network (CAN) and demonstrated it on the 2D XY model. The thermodynamics of the systems and the underlying Kosterlitz–Thouless transition were well recognized (see the lower panel of Fig. 4). Interestingly, by inspecting the output of the trained CAN on given XY spin configurations in the topological phase, it was found that the predicted conditional probabilities map matched automatically with the vorticity map of the configuration. This implied that perception of the topological vortex structure as the underlying effective degrees of freedom of the physical system naturally emerged from the trained network.

7.3 Application of Normalizing Flow. As another popular ML deep generative method, normalizing flow (NF) is currently under extensive exploration in the context of lattice QFT for phase transition studies. Being similar to the above-mentioned variational generative approach, NF uses neural networks to give a variational distribution that is implicitly constructed via an affine bijective function transformation represented by the network and exerted on a naive prior noise variable ($z \sim p(z)$) to generate the desired field configuration (ϕ): $\phi = g_\theta(z)$. Through the change of variable, the corresponding variational distribution under such an NF model is $p_\theta(\phi) = p(z)|\det(\frac{\partial z}{\partial \phi})|$. With a real NF with a volume-preserving structure to simplify the Jacobian determinant evaluation in the variational calculation, such flow-based models have been demonstrated for many different QFT systems,[59,60] including also the QCD system.[61] To alleviate the encountered multimode sampling difficulty, the Fourier transformation is introduced into the flow generative models and shown to be promising in generating Feynman paths for quantum systems.[62] This idea can be extended to explore phase transitions in various systems.

8. Summary. We have reviewed several phase transition studies that were enhanced by ML methods. Particular emphasis was placed on phase transitions within condensed matter, nuclear liquid–gas phase transitions, nuclear temperature determination and the identification of QCD transitions, as well as the inference of QCD EoS from high-energy HICs. We provide a succinct introduction to

several ML techniques deployed in these phase transition studies, demonstrating through these applications the capacity and invaluable insights ML offers for the exploration of intricate physics. Overall, discriminative learning algorithms such as the CNN, have shown promise in identifying phase transitions. Bayesian techniques provide a systematic way to unveil the thermodynamics related to phase transitions, while unsupervised deep generative AI models would facilitate non-perturbative exploration of phase transitions.

Acknowledgements. This work was partially supported by the National Natural Science Foundation of China (Grant Nos. 11890710, 11890714, and 12147101), and the BMBF funded KISS consortium (Grant No. 05D23RI1) in the ErUM-Data action plan.

References

[1] Aarts G *et al.* 2023 *Prog. Part. Nucl. Phys.* **133** 104070
[2] Bzdak A, Esumi S, Koch V, Stephanov M, and Xu N 2020 *Phys. Rep.* **853** 1
[3] Pochodzalla J, Möhlenkamp T, Rubehn T *et al.* 1995 *Phys. Rev. Lett.* **75** 1040
[4] Ma Y G 1999 *Phys. Rev. Lett.* **83** 3617
[5] Natowitz J B, Hagel K, Ma Y G *et al.* 2002 *Phys. Rev. Lett.* **89** 212701
[6] Natowitz J B, Wada R, Hagel K, Keutgen T, Murray M, Makeev A, Smith P, and Hamilton C 2002 *Phys. Rev. C* **65** 034618
[7] Ma Y G, Natowitz J B, Wada R *et al.* 2005 *Phys. Rev. C* **71** 054606
[8] Liu C, Deng X G, and Ma Y G 2022 *Nucl. Sci. Tech.* **33** 52
[9] Borderie B and Frankland J 2019 *Prog. Part. Nucl. Phys.* **105** 82
[10] Deng X G, Danielewicz P, Lin H, and Zhang Y X 2022 *Phys. Rev. C* **105** 064613
[11] Fukushima K and Hatsuda T 2011 *Rep. Prog. Phys.* **74** 014001
[12] Saiz A, García-Ramos J E, Arias J M, Lamata L, and Perez-Fernandez P 2022 *Phys. Rev. C* **106** 064322
[13] Li X B, Guo R R, Zhou Y *et al.* 2023 *Chin. Phys. C* **47** 034101
[14] He W B, Ma Y G, Pang L G, Song H C, and Zhou K 2023 *Nucl. Sci. Tech.* **34** 88
[15] Li F, Pang L G, and Wang X N 2023 *Nucl. Tech.* **46** 040014 (in Chinese)
[16] He W B, Li Q F, Ma Y G, Niu Z M, Pei J C, and Zhang Y X 2023 *Sci. China Phys. Mech. Astron.* **66** 282001
[17] Li P, Bai J H, Niu Z M, and Niu Y F 2022 *Sci. China Phys. Mech. Astron.* **52** 252006
[18] Wu Z H, Bai J J, Zhang D D *et al.* 2021 *Nucl. Sci. Tech.* **32** 54
[19] Liang J M, Wei S J, and Fei S M 2022 *Sci. China Phys. Mech. Astron.* **65** 250313
[20] Zhang Z Y, Ma R, Hu J F, and Wang Q 2022 *Chin. Phys. Lett.* **39** 111201
[21] Li Y Y, Zhang F, and Su J 2022 *Nucl. Sci. Tech.* **33** 135
[22] He L D, Guo H W, Jin Y B, Zhuang X Y, Rabczuk T, and Li Y 2022 *Sci. China Phys. Mech. Astron.* **65** 214612
[23] Li Z Y, Qian Z, He J H *et al.* 2022 *Nucl. Sci. Tech.* **33** 93
[24] Bai S C, Tang Y C, and Ran S J 2022 *Chin. Phys. Lett.* **39** 100701
[25] Ming X C, Zhang H F, Xu R R *et al.* 2022 *Nucl. Sci. Tech.* **33** 48
[26] Gao X, Sun J, Wan X G, and Li G 2022 *Chin. Phys. Lett.* **39** 077101
[27] Gao Z P, Wang Y J, and Lü H L *et al.* 2021 *Nucl. Sci. Tech.* **32** 109
[28] Arahmane H, Hamzaoui E M, Maissa Y B, and El Moursli R C 2022 *Nucl. Sci. Tech.* **32** 18
[29] Carrasquilla J and Melko R G 2017 *Nat. Phys.* **13** 431
[30] van Nieuwenburg E P L, Liu Y H, and Huber S D 2017 *Nat. Phys.* **13** 435
[31] Wetzel S J 2017 *Phys. Rev. E* **96** 022140
[32] Hu W J, Singh R R P, and Scalettar R T 2017 *Phys. Rev. E* **95** 062122
[33] Kelic A, Natowitz J B, and Schmidt K H 2006 *Eur. Phys. J. A* **30** 203
[34] Song Y D, Wang R, Ma Y G, Deng X G, and Liu H L 2021 *Phys. Lett. B* **814** 136084
[35] Ma Y G and Zhang S 2022 *Influence of Nuclear Structure in Relativistic Heavy-Ion Collisions.* In: Tanihata I, Toki H, and Kajino T (eds) *Handbook of Nuclear Physics* (Singapore: Springer) pp 1–30
[36] Wang Y Z, Zhang S, and Ma Y G 2022 *Phys. Lett. B* **831** 137198
[37] Wang S S, Ma Y G, He W B, Fang D Q, and Cao X G 2023 *Phys. Rev. C* **108** 014609
[38] Shi C Z and Ma Y G 2021 *Nucl. Sci. Tech.* **32** 66
[39] Ma Y G 2023 *Nucl. Tech.* **46** 080001 (in Chinese)
[40] Cao Y T, Deng X G, and Ma Y G 2023 *Phys. Rev. C* **108** 024610
[41] Wang R, Ma Y G, Wada R, Chen L W, Liu H L, and Sun K J 2020 *Phys. Rev. Res.* **2** 043202
[42] Wada R, Lin W, Ren P, Zheng H, Liu X, Huang M, Yang K, and Hagel K 2019 *Phys. Rev. C* **99** 024616
[43] Wu Y, Li X B, Chen L *et al.* 2023 *Nucl. Tech.* **46** 040006 (in Chinese)
[44] Zhang Y, Zhang D, and Luo X 2023 *Nucl. Tech.* **46** 040001 (in Chinese)
[45] Sun K J, Chen L W, Ko C M, Xu J, and Xu Z 2023 *Nucl. Tech.* **46** 040012 (in Chinese)
[46] Chen Q, Ma G L, and Chen J H 2023 *Nucl. Tech.* **46** 040013 (in Chinese)
[47] Pang L G, Zhou K, Su N, Petersen H, Stöcker H, and Wang X N 2018 *Nat. Commun.* **9** 210
[48] Du Y L, Zhou K, Steinheimer J, Pang L G, Motornenko A, Zong H S, Wang X N, and Stöcker H 2020 *Eur. Phys. J. C* **80** 516
[49] Steinheimer J, Pang L G, Zhou K, Koch V, Randrup J, and Stöcker H 2019 *J. High Energy Phys.* **2019** 122
[50] Kuttan M O, Zhou K, Redelbach A, and Stöcker H 2020 *J. High Energy Phys.* **2021** 184
[51] An R, Sun S, Cao L G, and Zhang F S 2023 *Nucl. Sci. Tech.* **34** 119
[52] Li P C, Wang Y J, Li Q F, and Zhang H F 2023 *Sci. China Phys. Mech. Astron.* **66** 222011
[53] Xu J F, Xia C J, Lu Z Y, Peng G X, and Zhao Y P 2022 *Nucl. Sci. Tech.* **33** 143
[54] Wang Y J, Li F P, Li Q F, Lü H L, and Zhou K 2021 *Phys. Lett. B* **822** 136669
[55] Kuttan M O, Steinheimer J, Zhou K, and Stöcker H 2023 *Phys. Rev. Lett.* **131** 202303
[56] Soma S, Wang L, Shi S, Stöcker H, and Zhou K 2023 *Phys. Rev. D* **107** 083028
[57] Zhou K, Endrődi G, Pang L G, and Stöcker H 2019 *Phys. Rev. D* **100** 011501
[58] Wang L X, Jiang Y, He L Y, and Zhou K 2022 *Chin. Phys. Lett.* **39** 120502
[59] Albergo M S, Kanwar G, and Shanahan P E 2019 *Phys. Rev. D* **100** 034515
[60] Kanwar G, Albergo M S, Boyda D, Cranmer K, Hackett D C,Racanière S, Rezende D J, and Shanahan P E 2020 *Phys. Rev. Lett.* **125** 121601
[61] Abbott R *et al.* 2023 *Prog. Sci.* **LATTICE2022** 036
[62] Chen S L, Savchuk O, Zheng S Q, Chen B Y, Stoecker H, Wang L X, and Zhou K 2023 *Phys. Rev. D* **107** 056001